

# Spectral and optoelectronic studies on 7,12,17-trioxa and 7,12,17-trithia [11] helicenes: a DFT view

N Islam and S S Chimni\*

Department of Chemistry, U.G.C. Centre of Advance Studies in Chemistry, Guru Nanak Dev University, Amritsar 143005, India

Received: 03 July 2016 / Accepted: 23 January 2017

**Abstract:** Density functional theory has been used to analyse the structural, spectral, charge transport and nonlinear properties of 7,12,17-trioxa [11] helicene and 7,12,17-trithia [11] helicene. The optimised geometries of TOH and TTH shows that carbon-carbon bond lengths of inner fused rings vary from terminal rings, as a consequence of generated torsional strain. The IR-spectra displays characteristics peaks in the region of 750–1550  $\text{cm}^{-1}$  in TOH and a slight shift occurs to lower frequency in case of TTH. The vibrational circular dichroism peaks have major contributions from in and out of plane bending and minor contribution from C=C stretching of fused aromatic rings. From ionisation and reorganization energy values it is evident that TOH and TTH can act as hole transport material for OLED device. As a consequence of extended conjugation in studied system, the higher values of polarizability and hyperpolarizability reflects their role in NLO devices.

**Keywords:** Chirality; Bond length alternation; Reorganisation energy; Polarizability; Transition dipole moment

**PACS Nos.:** 61.66.Hq; 31.15.E-; 34.70.+e; 42.65.-k; 33.20.Ea; 33.20.Vq

## 1. Introduction

Ortho-fused aromatic ring molecule usually acquires S-shape in order to release internal strain on account of distorted conjugated  $\pi$ -system. Thus helicenes are usually described as “molecules in distress”. These molecules are widely studied from last decades due to their unique properties originating from their helical system [1–3]. The steric interactions arising in these systems do not allow planarity for molecules cause the  $\delta$ -conjugated systems to get distorted into helices which gives rise to intrinsic chiral structures. These systems can wind in opposite directions and have a  $C_2$ -symmetric axis, which is perpendicular to the helical axis. This renders them chiral even though they have no asymmetric carbons or other chiral centres [4, 5]. On the basis of the helicity rule proposed by Cahn et al. [6], a left-handed helix is designated “minus” and denoted by  $M$  whereas a right-handed one is designated “plus” and

denoted by  $P$  (Fig. 1). Inherited molecular chirality in helicenes give rise to interesting electronic and optical properties which defines their role in molecular wires, organic light emitting devices and solar cells [7–14]. These molecules forms helical columnar motifs which makes them potential applicant for nonlinear optical and circularly polarised light emitting material. Due to extended  $\pi$ -electron cloud these compounds display circular dichroism, exhibiting large second order nonlinear optical response (NLO) and can be used in liquid crystal displays [15–19].

Mainly there are two types of helical molecules: carbahelicenes and heterohelicenes. The carbahelicence are widely synthesized and explored for their electronic and nonlinear optical properties [20–25]. The presence of heteroatoms in the helicene backbone significantly alters both the molecular and the self-assembly properties of helical polyaromatics [26–29]. Thiophenes in thiohelicenes (containing alternate thiophene and benzene rings) are modules expected to determine desirable effects in these systems. Indeed thiohelicenes are stable materials which can be synthesized in good yields via photochemical irradiation using either standard laboratory equipment or solar powered reactors [30, 31]. Recently tremendous focus is concentrated on the design of helicenes for tuning and exploring their

**Electronic supplementary material** The online version of this article (doi:10.1007/s12648-017-1000-8) contains supplementary material, which is available to authorized users.

\*Corresponding author, E-mail: sschimni@yahoo.com; sschimni.chem@gndu.ac.in

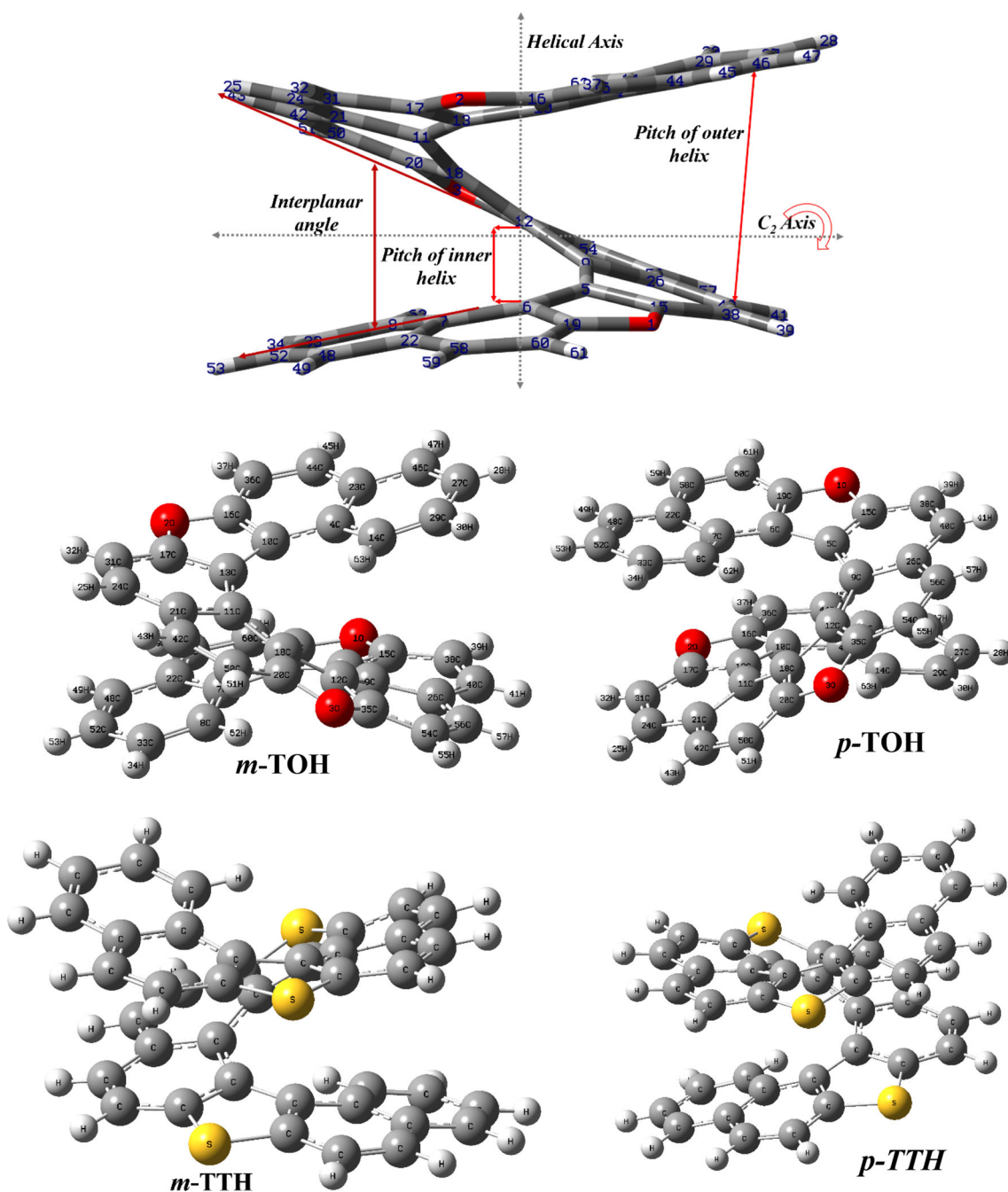


**Fig. 1** Lowest energy optimized geometries of *m* and *p* atropisomers of 7,12,17-trioxa (TOH) and 7,12,17-trithia [11] (TTH) helicenes

much promising electronic properties on introducing hetero atoms in helical chain. Researcher have observed that low lying energy level of heterohelicenes particularly fused furans are known to show interesting utility in electronic devices as organic light-emitting diodes or organic field-effect transistors [32–37]. However the increase in internal strain on adding fused rings creates difficulties in synthesis of larger helicenes. The [14] helicenes, [16] helicene, hexathia [13] helicene, [11] helicene, poly(thia-heterohelicene) are the largest helices reported in the literature till this date [1, 2].

The compounds belonging to the general class of oxa-helicenes and thia-helicenes have been synthesized, and their various properties have been studied [38–45]. Recently Sundar and Bedekar [46] reported the design and synthesis of oxygen-containing 7,12,17-trioxa [11] helicene. However the vibrational circular dichroism and optoelectronic properties of these helicene have not been reported so far. The main objective of this study is to provide a complementary understanding of chiral and optoelectronic behaviour of the trioxa-(TOH) and trithia-(TTH) helical systems.

## 2. Computational method

All calculations in this work were performed by using the Gaussian 09 program package [47]. The original structure of TOH synthesized by Sundar and Bedekar [46] were obtained through CCDC database, then the modified geometries were optimized at the density functional theory (DFT) level using CAM-B3LYP functional in conjunction with 6-311++G (2d, 2p) basis set in the gas phase [48, 49]. The geometry of TTH was directly designed using graphical software Gauss view and then optimised at the same level of theory as employed for TOH [50]. All the optimized geometries were examined by frequency calculations to ensure them as true minima. The neutral molecules were treated as closed-shell systems; while for the radical anion and radical cation open-shell system optimizations were carried out using a spin unrestricted wave function (UCAM-B3LYP procedure). For gaining more insights into the excited states properties (excitation energies, transition dipole moment and rotatory strengths) of studied systems, adiabatic approximation using time-dependent density functional theory (TD-DFT) calculations at CAM-B3LYP/6-311G++(2d, 2p) level were invoked to simulate the lower excited states [51]. The CAM-B3LYP functional was

employed as the results obtained from this basis functional are usually in line with the experimental findings. The solvent effect on the absorption spectra was addressed by employing IEFPCM solvent model [52–55]. IEFPCM model implements a self-consistent reaction field method; the integral equation formalism polarisable continuum model, in which the solvent is considered as a continuum of a determined dielectric constant and the solute is within a cavity of the solvent and is modelled as a series of interlocked spheres.

## 3. Result and discussion

### 3.1. Molecular geometry

The optimized molecular geometry of TOH and TTH have been calculated using DFT/CAM-B3LYP method with 6-311G++(2d, 2p) basis set and the geometry of molecules with labelling of atoms is shown in Fig. 1. The calculated structural parameters of the TOH molecule are listed in Table 1 and these parameters are found to be in close agreement with crystal data [46]. The slight deviations observed may be attributed to the fact that theoretical

**Table 1** Comparison of geometrical parameters of DFT optimised and experimental obtained structure of *m*-TOH helical system

Bond	Gaussian	Experiment <sup>a</sup>	Angle	Gaussian	Experiment <sup>a</sup>
C <sub>4</sub> –C <sub>14</sub>	1.409	1.405	C <sub>14</sub> C <sub>4</sub> C <sub>10</sub>	124.06	123.92
C <sub>14</sub> –C <sub>29</sub>	1.369	1.369	C <sub>10</sub> C <sub>13</sub> C <sub>11</sub>	136.17	135.93
C <sub>29</sub> –C <sub>27</sub>	1.406	1.398	C <sub>13</sub> C <sub>11</sub> C <sub>18</sub>	137.11	137.87
C <sub>27</sub> –C <sub>46</sub>	1.362	1.360	C <sub>11</sub> C <sub>18</sub> C <sub>12</sub>	129.01	128.22
C <sub>46</sub> –C <sub>23</sub>	1.414	1.414	C <sub>18</sub> C <sub>12</sub> C <sub>9</sub>	137.43	138.31
C <sub>23</sub> –C <sub>4</sub>	1.424	1.427	C <sub>12</sub> C <sub>9</sub> C <sub>5</sub>	137.49	138.39
C <sub>4</sub> –C <sub>10</sub>	1.431	1.431	C <sub>9</sub> C <sub>5</sub> C <sub>6</sub>	129.79	129.27
C <sub>10</sub> –C <sub>13</sub>	1.458	1.452	C <sub>5</sub> C <sub>6</sub> C <sub>7</sub>	137.56	138.17
C <sub>13</sub> –C <sub>17</sub>	1.387	1.392	C <sub>6</sub> C <sub>7</sub> C <sub>8</sub>	124.06	125.13
C <sub>17</sub> –O <sub>2</sub>	1.359	1.367	C <sub>19</sub> OC <sub>15</sub>	105.97	105.30
O <sub>2</sub> –C <sub>16</sub>	1.362	1.370	C <sub>35</sub> O <sub>3</sub> C <sub>20</sub>	106.03	105.49
C <sub>13</sub> –C <sub>11</sub>	1.428	1.431	C <sub>17</sub> O <sub>2</sub> C <sub>16</sub>	105.93	105.19
C <sub>11</sub> –C <sub>18</sub>	1.428	1.434	C <sub>14</sub> C <sub>13</sub> C <sub>9</sub>	53.53	53.51
C <sub>18</sub> –C <sub>12</sub>	1.469	1.471	C <sub>13</sub> C <sub>9</sub> C <sub>7</sub>	55.12	55.18
C <sub>12</sub> –C <sub>35</sub>	1.388	1.395			
C <sub>35</sub> –O <sub>3</sub>	1.362	1.360			
O <sub>3</sub> –C <sub>20</sub>	1.362	1.367			
C <sub>12</sub> –C <sub>9</sub>	1.428	1.437			
C <sub>9</sub> –C <sub>5</sub>	1.428	1.429			
C <sub>5</sub> –C <sub>6</sub>	1.458	1.461			
C <sub>6</sub> –C <sub>19</sub>	1.382	1.382			
C <sub>19</sub> –O <sub>1</sub>	1.362	1.374			
O <sub>1</sub> –C <sub>15</sub>	1.359	1.363			

<sup>a</sup> Ref. [46]

calculations are done for single isolated molecule in gaseous phase and the experimental values are those from of the crystalline solid phase. This indicated that the adopted density functional and basis set are feasible for the studied systems. The calculated geometrical parameters of TOH and TTH shows that C–C and C=C bond lengths of the inner fused rings vary from the peripheral rings, as a consequence of generated torsional strain. While comparing the C–C bond length of TTH and TOH with benzene (1.393 Å) the inner helix is slightly lengthened and outer ones are close to benzene. It is also interesting to see the difference between the bond lengths of the heteroatom fused furan and thio rings. The bond length of the peripheral furan or thiophene rings are almost same how're, the central furan or thiophene ring is found to be slightly elongated due to much greater strain exerted in the inner portion. Thus the studied helicenes show deviation from  $C_2$  symmetry due to different bonds lengths and the torsion angles between the inner carbons. The interplanar angles for TOH and TTH are found 25.01° and 25.68° which agrees well with the experimental reported for TOH helicene. For the studied TOH (TTH) the inner pitch opts a value of 3.331 Å (3.412 Å) and outer pitch of 4.799 Å (4.803 Å) respectively. In order to account for the local aromaticity change we have calculated BLA (bond length alternation) values associated with the  $C_5-C_9$ ,  $C_9 = C_{26}$ ,  $C_{26}-C_{40}$ ,  $C_9-C_{12}$ ,  $C_{12} = C_{35}$  and  $C_{35}-O/C_{35}-S$ . According the Fu et al. [56] BLA is calculated by subtracting the arithmetic mean of the two central C–C bonds and the central C=C bond length and given as

$$BLA = \frac{d(C_9-C_{12}) + d(C_{35}-S/O)}{2} - d(C_{12} = C_{35}) \quad (1)$$

The BLA value obtained by employing  $C_5-C_9$ ,  $C_9 = C_{26}$ ,  $C_{26}-C_{40}$  is 0.221 and 0.197 for TOH and TTH respectively. However on employing  $C_9-C_{12}$ ,  $C_{12} = C_{35}$  and  $C_{35}-O/C_{35}-S$  bond lengths BLA value for TOH and TTH is 0.213 and 0.194, respectively. These observations have revealed that in TOH and TTH system the aromaticity of inner rings are effected more as compared to peripheral rings. However TTH displays enhanced extension in conjugation on account of effective delocalisation of lone pair present on the sulphur with the  $\pi$ -electron of fused system with results in increased double character of C–C bonds.

## 3.2. Vibrational assignment

### 3.2.1. IR and VCD spectra

The molecules TOH and TTH consists of 63 atoms and belongs to C1 point group. These molecules adopts non-planar geometry inherited from helical framework.

Therefore, all the 183 vibrational modes of TOH and TTH are active in both IR and Raman spectra. The simulated vibrational spectra for TOH and TTH are given in Fig. 2. Vibrational analysis is carried to find vibrational modes connected with specific molecular structures of calculated helical system. DFT levels give vibrational spectrum with high accuracy relative to experimental spectrum. However, it should be noted that the DFT calculations are performed for a free molecule in vacuum, while experiments are carried out on solid samples which expose them to different intra- and inter-molecular interactions. In addition, DFT calculations give higher wavenumbers than experimental ones due to negligence of anharmonicity, incomplete inclusion of electron correlation effects and basis set deficiencies. Therefore, the calculated vibrational wavenumbers of TOH and TTH have been scaled down by 0.95 to get more reliable values. The IR absorption peaks obtained in the region of 750–3100  $\text{cm}^{-1}$  (see Fig. 2) are due to excitation of normal modes at 753.16  $\text{cm}^{-1}$  (750.91  $\text{cm}^{-1}$ ), 798.24  $\text{cm}^{-1}$  (786.13  $\text{cm}^{-1}$ ), 958.15  $\text{cm}^{-1}$  (941.65  $\text{cm}^{-1}$ ), 1040.71  $\text{cm}^{-1}$  (–), 1175.63  $\text{cm}^{-1}$  (1161.32  $\text{cm}^{-1}$ ), 1213.16  $\text{cm}^{-1}$  (1209.11  $\text{cm}^{-1}$ ), 1326.04  $\text{cm}^{-1}$  (–), 1503.43  $\text{cm}^{-1}$  (1501.14  $\text{cm}^{-1}$ ), 1557.67  $\text{cm}^{-1}$  (1551.98  $\text{cm}^{-1}$ ) and 3033.12  $\text{cm}^{-1}$  (3027.75  $\text{cm}^{-1}$ ) for TOH (TTH). The first three absorptions (750–956  $\text{cm}^{-1}$ ) have contribution from out-of-plane CH stretching of aromatic rings while as 1040.71  $\text{cm}^{-1}$  (–), 1175.63  $\text{cm}^{-1}$  (1161.32  $\text{cm}^{-1}$ ), 1213.16  $\text{cm}^{-1}$  (1209.11  $\text{cm}^{-1}$ ) and 1326.04  $\text{cm}^{-1}$  (–) are attributed to CH in plane bending vibrations of aromatic rings. In addition to these peaks the TOH (TTH) shows additional peaks at 1503.43  $\text{cm}^{-1}$  (1501.14  $\text{cm}^{-1}$ ), 1557.67  $\text{cm}^{-1}$  (1551.98  $\text{cm}^{-1}$ ) due to the C=C stretching vibrations of fused aromatic rings. In our calculations, aromatic CH stretching vibrations are assigned at the range

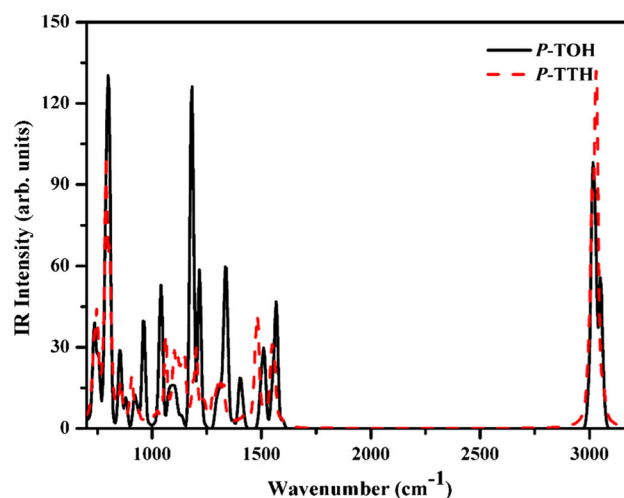


Fig. 2 IR spectral intensity (900–3200  $\text{cm}^{-1}$  region) of *m*-atropisomer of TOH and TTH. A scale factor of 0.95 is used

of 3011–3038 and 3013–3045  $\text{cm}^{-1}$  for TOH and TTH with an intense peaks at 3013 and 3039  $\text{cm}^{-1}$ , respectively. The IR wavenumbers are found in close agreement with experimental reported for aromatic systems. However, in case of TTH the peaks in the mid IR region are not fully resolved but the intensity of the peak increased in 3013–3045  $\text{cm}^{-1}$  region.

The VCD spectra (see Fig. 3(a)) of *M*-TOH and *P*-TOH configurations show intense VCD peaks with opposite polarization at 950.13 and 1310.51  $\text{cm}^{-1}$ . The VCD signal for *M*-TOH isomer (*P*-TOH isomer) has positive (negative) polarization at 950.13 and 1310.51  $\text{cm}^{-1}$  and negative (positive) polarization at 1033.17  $\text{cm}^{-1}$ . These intense peaks arise from in-plane and out of plane bending modes of vibrations which can be effectively used as a configuration markers. The less prominent VCD peaks at 1418.56  $\text{cm}^{-1}$  and 1488.74  $\text{cm}^{-1}$  display positive polarization for *M*-1 with change in polarization at 1457.34  $\text{cm}^{-1}$ . In the CH stretching region a doublet with low intensity having positive polarization for *M*-TOH atropisomer has appeared. We have observed that the VCD spectra for TTH moiety is much resolved as compared to the TOH. VCD spectra for *M*-TTH and *P*-TTH (see Fig. 3(b)) display two prominent peaks at 905.71 and 1546.55  $\text{cm}^{-1}$  showing left polarization for *M*-TTH. The spectra appears with three doublets at 1021.63, 1337.21 and 1485.76  $\text{cm}^{-1}$  which can be good marker of the chiral configuration for atropisomers of TTH. Among these doublets, the first and third shows negative polarization while the middle one shows positive for *M*-TTH with change in polarization at 1301.56 and 1398.11  $\text{cm}^{-1}$  respectively. The enhanced polarization in *M*-TTH and *P*-TTH is due to the presence of large sulphur atom which allows the effective relaxation of normal modes. In addition, the VCD spectra of TTH displays a well resolved

doublet at 3011.68  $\text{cm}^{-1}$  with negative polarization for *M*-TTH in the CH aromatic stretching region of the helicene.

### 3.3. Frontier molecular orbitals, UV–visible spectra, charge transfer and nonlinear response

The components and energies of the frontier molecular orbitals are very important to investigate the trend in charge transfer and nonlinear optical properties. The stereo contour graphs of the frontier molecular orbitals of the TOH and TTH in neutral, anionic and cationic states are shown in Fig. 4. From Fig. 4, we can see that although the component characteristics of the frontier molecular orbitals of the two helicenes are same in electron density distribution, but they displays differences in their charged states. The highest occupied molecular orbitals of TOH and TTH in neutral are mainly concentrated over terminal aromatic rings including the heteroatoms and lowest unoccupied distributed over the mid-fused aromatic rings. The HOMO-1 in both cases resembles with the HOMO distribution but have increased electron density over the heteroatoms. However in case of LUMO + 1 the electron density is focussed over helical framework excluding the heteroatoms. Thus, the first the excitation will originate both from HOMO-1 and HOMO orbitals including  $n \rightarrow \pi^*$  and  $\pi \rightarrow \pi^*$  transitions. In case of ionic states, the HOMO and LUMO displays increased electron density in the terminal and fused aromatic rings respectively. The HOMO-1 in anionic states shows more electron density over the heteroatoms as compared to cationic state. Thus, in the charged state the transition will be mainly  $\pi \rightarrow \pi^*$  in cationic state and  $n \rightarrow \pi^*$  in case of anionic geometry of TOH or TTH. Such characteristics of the frontier molecular orbitals can be used to explain the nature of charge transfer over oxidation or reduction of the helical systems. Thus, in

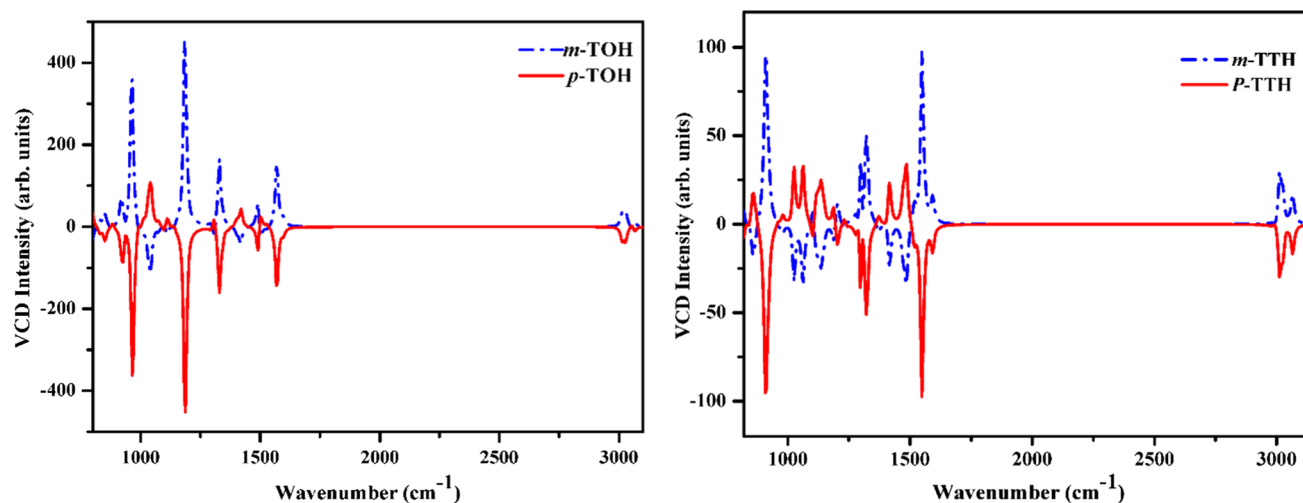
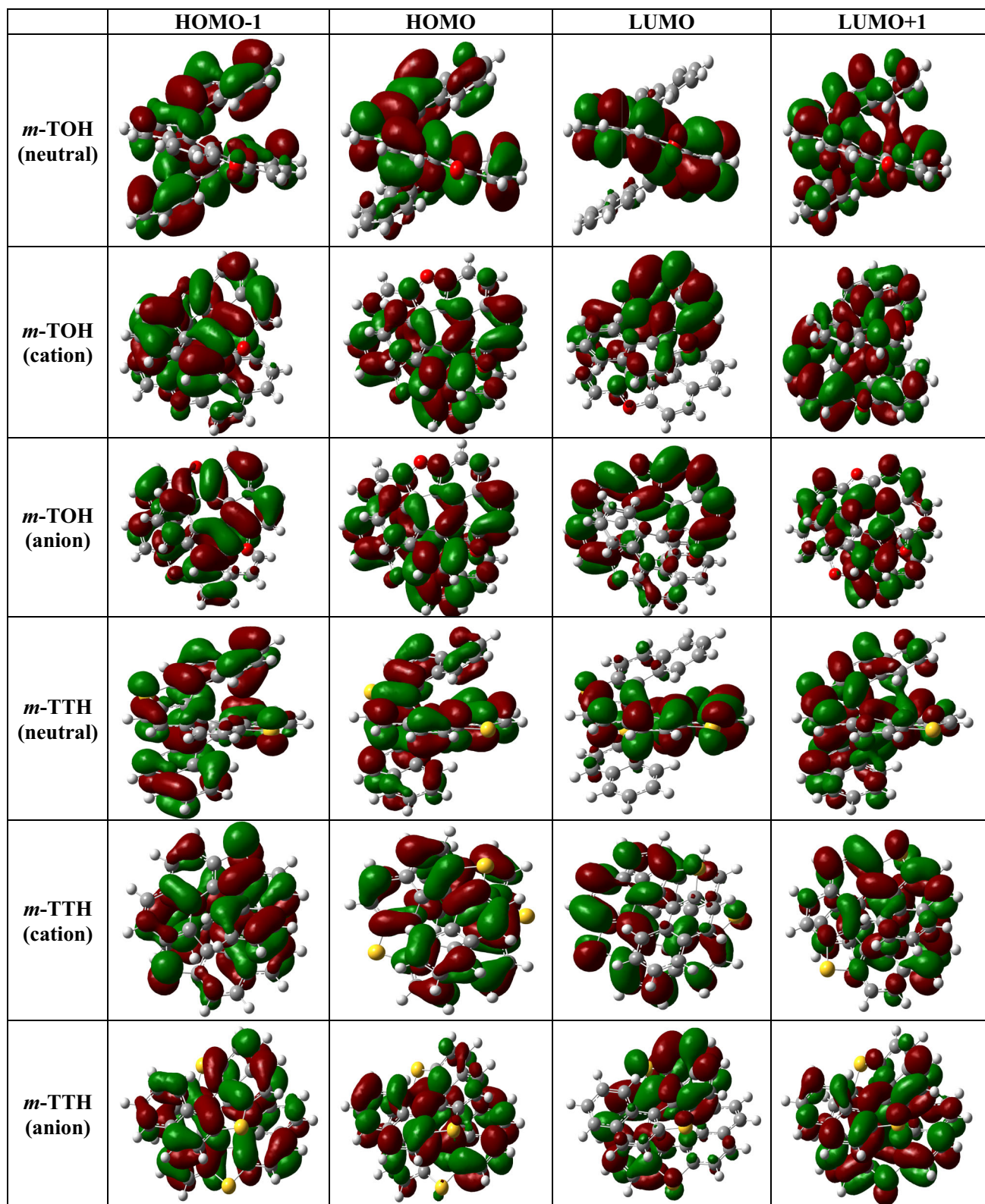


Fig. 3 VCD spectral intensity (900–3200  $\text{cm}^{-1}$  region) of atropisomers of TOH and TTH. A scale factor of 0.95 is used



**Fig. 4** FMO of the TOH and TTH in neutral, cationic and anionic states calculated at DFT level of theory

order to understand the electronic absorption behaviour, we have employed TD-TDFT/CAM-B3LYP level of theory for simulation of electronic states in gas phase as well as in

solvent using IEFPCM model. The calculated excitation energies, oscillator strength, transition dipole moment and orbital contribution for TOH and TTH are given Table 2.

**Table 2** Results of TDFT calculations at CAM-B3LYP/6-311G++(2d, 2p) level of theory for the electronic transitions of helical systems

States	Excitation	$\lambda^a$	$f^b$	Td <sup>c</sup>	Orbital contribution
<i>m</i> -TOH					
S1(gas)	3.489	352.32	0.064	3.207	<i>HOMO</i> → <i>LUMO</i> (84%)
S2(gas)	3.533	350.86	0.152	2.169	<i>HOMO</i> → <i>LUMO</i> + 1(80%)
S3(gas)	3.702	334.87	0.233	2.099	<i>HOMO</i> -1 → <i>LUMO</i> (76%)
S1(water)	3.118	397.60	0.102	2.216	<i>HOMO</i> → <i>LUMO</i> (86%)
S2(water)	3.218	385.20	0.218	1.643	<i>HOMO</i> → <i>LUMO</i> + 1(80%)
S3(water)	3.284	377.54	0.325	3.485	<i>HOMO</i> -1 → <i>LUMO</i> (73%)
S1(acetonitrile)	3.201	387.37	0.103	2.327	<i>HOMO</i> → <i>LUMO</i> (84%)
S2(acetonitrile)	3.448	381.53	0.221	1.734	<i>HOMO</i> → <i>LUMO</i> + 1(80%)
S3(acetonitrile)	3.474	356.12	0.326	3.396	<i>HOMO</i> -1 → <i>LUMO</i> (77%)
S1(cyclohexane)	3.169	391.24	0.106	2.085	<i>HOMO</i> → <i>LUMO</i> (86%)
S2(cyclohexane)	3.308	374.83	0.241	1.260	<i>HOMO</i> → <i>LUMO</i> + 1(82%)
S3(cyclohexane)	3.469	357.31	0.337	3.089	<i>HOMO</i> -1 → <i>LUMO</i> (74%)
<i>m</i> -TTH					
S1(gas)	3.477	364.32	0.071	2.403	<i>HOMO</i> → <i>LUMO</i> (63%)
S2(gas)	3.509	353.74	0.193	1.981	<i>HOMO</i> → <i>LUMO</i> + 1(76%)
S3(gas)	3.683	341.59	0.256	2.171	<i>HOMO</i> -1 → <i>LUMO</i> (60%)
S1(water)	3.016	399.01	0.093	2.234	<i>HOMO</i> → <i>LUMO</i> (61%)
S2(water)	3.119	387.91	0.107	1.165	<i>HOMO</i> → <i>LUMO</i> + 1(79%)
S3(water)	3.255	380.77	0.198	2.571	<i>HOMO</i> -1 → <i>LUMO</i> (59%)
S1(acetonitrile)	3.319	391.34	0.053	2.091	<i>HOMO</i> → <i>LUMO</i> (62%)
S2(acetonitrile)	3.312	374.35	0.021	1.269	<i>HOMO</i> → <i>LUMO</i> + 1(79%)
S3(acetonitrile)	3.471	357.21	0.125	3.076	<i>HOMO</i> -1 → <i>LUMO</i> (58%)
S1(cyclohexane)	3.072	403.16	0.058	2.235	<i>HOMO</i> → <i>LUMO</i> (66%)
S2(cyclohexane)	3.139	394.87	0.016	1.166	<i>HOMO</i> → <i>LUMO</i> + 1(79%)
S3(cyclohexane)	3.256	380.74	0.310	3.923	<i>HOMO</i> -1 → <i>LUMO</i> (62%)

<sup>a</sup> Wavelength<sup>b</sup> Oscillatory frequency<sup>c</sup> Transition dipole moment

The calculated values display a very strong maximum absorption peak at 352 nm and 364 nm for TOH and TTH in vacuo. It is also noteworthy that the maximum absorption peaks of both the TTH show the bathochromic shift as compared to TOH possibly due to enhanced conjugated system on account of less electronegativity of sulphur. The comparison of the simulated spectral data in acetonitrile for TOH are in good agreement with experimental spectrum [46], thus validating the selected basis set employed in our calculation. Inclusion of solvation effects introduces relevant changes in the maximum absorption and oscillatory strength with respect to that computed in vacuo. Both the helical systems displays bathochromic shift together with an increasing intensity (oscillatory strength) but more prominent in non-polar solvent (cyclohexane) and less prominent in polar solvents (water and acetonitrile). We have noted that in both cases, the first three transitions originating from *HOMO* → *LUMO*, *HOMO*-1 → *LUMO*

and *HOMO* → *LUMO* + 1 displays significant value for oscillatory strength with prominent change in dipole moment upon transitions.

In order to quantify the stability and charge transfer properties, we have calculated all the corresponding quantum mechanical descriptors and reorganisation energies values for TOH and TTH helical system. The vertical and adiabatic ionisation potential and electronic affinity of helical systems are calculated by using equations and are given in Table 3

$$IP(v)/IP(a) = E^+(M)/E^+(M^+) - E(M) \quad (2)$$

$$EA(v)/EA(a) = E(M) - E^-(M)/E^-(M^-) \quad (3)$$

where  $IP(v)/IP(a)$  and  $EA(v)/EA(a)$  are vertical and adiabatic ionisation potential and electron affinity respectively.  $E(M)$ ,  $E^+(M^+)$ , and  $E^-(M^-)$  are the respective energies of optimized neutral, cationic, and anionic structures.  $E(M^+)/E(M^-)$  is the neutral energy of the optimized

**Table 3** HOMO, LUMO, reorganisation energy, ionisation potential and electron affinity calculate at CAM-B3LYP/6-311G++(2d, 2p) level of theory

	HOMO (eV)	LUMO (eV)	$\Delta E$	$\lambda_h$	$\lambda_e$
<i>m</i> -TOH	-6.438	-3.429	3.009	0.130	0.186
<i>m</i> -TTH	-6.356	-3.289	3.067	0.108	0.157
	IP	$EA(v)/EA(a)$	$\eta$	$\mu$	$\omega$
<i>m</i> -TOH	6.17	1.412/1.381	4.934	-1.505	5.584
<i>m</i> -TTH	6.24	1.481/1.464	4.822	-1.534	5.673

cationic/anionic structure and  $E^+(M)/E(M^-)$  is the cationic/anionic energy of the optimized neutral structure.

The chemical hardness, chemical potential and electrophilicity index are calculated by employing Koopmans' theorem i.e., ionisation energy and electron affinity are the eigenvalue of the HOMO and LUMO with change of sign [57].

To calculate the rate of charge transfer ( $k_{et}$ ) we have applied standard Marcus electron-transfer theory for deriving reorganisation energy corresponding to hole or electron transfer [58, 59].

$$k_{et} = \left(4\pi^2/h\right) \Delta H_{ab}^2 (4\pi\lambda k_B T)^{-1/2} \exp\left(-(\Delta G^0 + \lambda)^2 / 4\lambda k_B T\right) \quad (4)$$

where  $\lambda$  and  $\Delta H_{ab}$  are the reorganization energy for the intramolecular electron transfer and the electronic coupling integral between donor-acceptor pair, respectively, and  $\Delta G^0$  is the Gibbs free energy change of the process.

The reorganisation energy is the energy dissipated when a system has undergone vertical electron transfer relaxes to the equilibrium geometry for its new charge distribution. From the Eq. 4, it is clear that  $\lambda$  should be low to get a high electron or hole transfer rate. The intramolecular reorganisation energy for hole and electron transport is calculated by using Eqs. (5) and (6) corresponding to the relaxation energies upon going from neutral state to charged geometry and vice versa.

$$\lambda_h = [E(M^+)] - [E(M)] + [E^+(M) - E^+(M^+)] \quad (5)$$

$$\lambda_e = [E(M^-)] - [E(M)] + [E^-(M) - E^-(M^-)] \quad (6)$$

The calculated values of intramolecular reorganisation energies for TOH and TTH are given in Table 3. We have observed that  $\lambda_h$  (reorganisation energy for hole transport) values are comparatively smaller as compared to the  $\lambda_e$  (reorganisation energy for electron transport) values demonstrating relevance of studied helical derivatives as p-type material for Organic Light Emitting devices.  $\lambda_h$  for TOH and TTH molecules are found lower than those reported for triarylamine helical systems [36]. Lin et al. [60], have calculated the reorganization energies of Alq3 for hole and electron transport to be 0.242 and 0.276 eV,

respectively. Thus, the lower value of  $\lambda_h$  and  $\lambda_e$  for studied system as compared to Alq3 display their possible applications in electronic devices. The theoretically calculated  $EA(a)$  for the molecular oxygen at the B3LYP/6-31G+ is 0.59 eV [61], while the experimental value, determined by photoelectron spectroscopy is reported as  $0.448 \pm 0.006$  eV [62]. The calculated  $EA(a)$  values for the TOH and TTH are greater than 1.0 eV defining their anionic stability towards the oxygen and water in air. The effect of heteroatom on the electronic properties of helical system are viewed in terms of IP or EA or electrophilicity index. The TOH displays higher values of IP and EA and lower value of electrophilicity index due to higher electronegativity of oxygen as compared to sulphur atom. The higher value for EA and IP value shows that the holes can be consequently injected into the emissive layer much more easily in case of TOH as compared to TTH. Thus, by combining the relationships between IP values and presence of low lying HOMO and LUMO energy level signifies that the studied helical systems possess high oxidation and reduction stabilities. On relating our findings with review reported by Sasabe and Kido [63] the helical systems can be applicable as hole transport material with the work function of the metal electrode like ITO ( $\Phi = -4.70$ ) used in practical OLED devices.

In this study we have calculated electronic dipole moment, molecular polarizability, anisotropy of polarizability ( $\alpha$ ), first hyperpolarizability ( $\beta$ ) and second hyperpolarizability ( $\gamma$ ) using DFT/CAM-B3LYP/6-311G++(2d, 2p) level of theory. Polarizability and hyperpolarizability characterises the response of a system in an applied field. It is well known for various studies that the molecular polarizability, hyperpolarizability and dipole moments are important for active nonlinear performance of the chemical system [64, 65]. Helical system (TOH and TTH) contained  $sp^2$ -hybridised carbon, the electron in the  $p_z$ -orbital of each  $sp^2$ -hybridised carbon atom will form  $\pi$ -bonds with the neighbouring  $p_z$ -electrons. These  $\pi$ -electrons are of a delocalised nature, resulting in high electronic polarizability. This has also been reflected from the obtained higher polarizability value of TTH as compared to TOH resulted from more effective  $\pi$ -conjugation on account less electronegativity of sulphur atom. The polarizability and hyperpolarizability are quantified by employing finite field (FF) method. In finite field (FF) method, when a molecule is subjected to a static field (F), the energy (E) of the molecule is expressed as:

$$E = E^0 - \mu_i F_i - \frac{1}{2} \alpha_{ij} F_i F_j F_k - \frac{1}{24} \gamma_{ijkl} F_i F_j F_k F_l - \quad (7)$$

where  $E^0$  is the energy of the molecule in the absence of electronic field,  $\mu$  is a component of the dipole moment vector given as:

**Table 4** Calculated values of dipole moment, polarizability, anisotropy in polarizability and hyperpolarizability for m-TOH and m-TTH helical systems

	$\mu$ (debye)	$\alpha$ ( $\times 10^{-24}$ esu.)	$\Delta\alpha$	$\beta$ ( $\times 10^{-32}$ esu.)	$\gamma$ ( $\times 10^{-34}$ esu.)
m-TOH	0.527	62.397	79.45	119.889	-0.674
m-TTH	0.573	67.719	84.15	166.822	-0.631

$$\mu = \left( \mu_x^2 + \mu_y^2 + \mu_z^2 \right)^{1/2} \quad (8)$$

$\alpha$  is the linear polarizability tensor,  $\beta$  and  $\gamma$  are the first and second hyperpolarizability tensors and i, j and k are labels for x y and z components respectively and are given as

$$\alpha = 1/3(\alpha_{xx} + \alpha_{yy} + \alpha_{zz}) \quad (9)$$

$$\beta = \left[ (\beta_{xxx} + \beta_{xyy} + \beta_{xzz})^2 + (\beta_{yyy} + \beta_{yzz} + \beta_{yxx})^2 + (\beta_{zzz} + \beta_{zxx} + \beta_{zyy})^2 \right]^{1/2} \text{ or } \beta = \left[ \beta_x^2 + \beta_y^2 + \beta_z^2 \right]^{1/2} \quad (10)$$

where  $\beta_x^2$ ,  $\beta_y^2$  and  $\beta_z^2$  are the components of the second order polarizability tensors and can be calculated by using equations:

$$\beta_i = \beta_{iii} + \frac{1}{3} \sum_{i \neq j} [(\beta_{ijj} + \beta_{jij} + \beta_{jji})], i, j, = x, y, z \quad (11)$$

and

Average value of third order hyperpolarizability is given as

$$\langle \gamma \rangle = \frac{1}{5} [\gamma_{xxxx} + \gamma_{yyyy} + \gamma_{zzzz} + 2[\gamma_{xyyy} + \gamma_{yyzz} + \gamma_{xxzz}]] \quad (12)$$

The calculated polarizability and first order hyperpolarizability of TOH and TTH have significant higher values to define their role in NLO device (Table 4). Comparison between the two studied helical systems shows that decrease in electronegativity of heteroatom increases the nonlinear activity of the helicene. On comparing the hyperpolarizability values with reorganisation energy values of TOH and TTH, we observe an inverse relation i.e. hyperpolarizability display increase with decrease in value of both  $\lambda_e$  and  $\lambda_h$ . The enhancement of  $\beta$  value for TTH as compared TOH also correlated with increased  $u_{ge}$  and decreased excitation energy of former as compare to later, thus following the Oudar and Chemla two level model [66]. It is worth noting that TOH and TTH helical systems shows higher value of second order hyperpolarizability as compared to already used material for NLO devices [36, 67]. In addition to it the effective  $\pi$ -conjugation in TOH and TTH helical will cause ring current in these system, thus will display NLO activity even in absence of external field. Therefore, the studied

helical system will be prone to be effective material for the nonlinear devices.

#### 4. Conclusion

In this study molecular structure, spectral (IR, VCD and UV-visible), charge transport and nonlinear optical properties are calculated for TOH and TTH using CAM-B3LYP/6-311G++(2d, 2p) level of theory. We have observed small differences between the theoretical and experimental structural parameters and vibrational wavenumbers. The wavenumbers corresponding to bending and stretching modes of aromatic rings are found to be good configurational markers. From FMO analysis, we have observed that the electron density of the two helicenes defines similar pattern, however shows difference in their charged states. The absorption maximum shifts towards higher wavelengths on employing solvent medium particularly in case of non-polar solvent (cyclohexane). The calculated ionisation energy, electron affinity and reorganisation energy values of TOH and TTH describe them as hole transport material for OLED. TOH and TTH opts sufficient values of adiabatic electron affinity for defining their stability against moisture and molecular oxygen. Nonlinear optical behaviour of the examined systems are investigated by the determination of the electric dipole moment, the polarizability and hyperpolarizability values. The calculated values of  $\alpha$ ,  $\beta$  and  $\gamma$  of the two helicenes are found on the higher side as compared to the molecules already reported in literature for NLO activity. So, it is demonstrated that the investigated helicenes can be used as a NLO material.

**Acknowledgements** NI is thankful to University Grants Commission (UGC) India, for providing financial support through Dr D. S. Kothari postdoctoral fellowship (Grant No. F.4-2/2006 (BSR)/CH/13-14/0126).

#### References

- [1] M Gingras *Chem. Soc. Rev.* **42** 968 (2013)
- [2] M Gingras G Felix and R Peresutt *Chem. Soc. Rev.* **42** 1007 (2013)
- [3] M Gingras *Chem. Soc. Rev.* **42** 1051 (2013)

- [4] S Grimme, J Harren, A Sobanski and F Vögtle *Eur. J. Org. Chem.* **1998** 1491 (1998)
- [5] Y Shen and C F Chen *Chem. Rev.* **112** 1463 (2012)
- [6] R S Cahn, C Ingold and V Prelog *Angew. Chem., Int. Ed.* **5** 385 (1966)
- [7] R Hassey, E J Swain, N I Hammer, D Venkataraman and M D Barnes *Science* **314** 1437 (2006)
- [8] R Hassey, K D McCarthy, E S D Basak, D Venkataraman and M D Barnes *Chirality* **20** 1039 (2008)
- [9] Y Q Tang, T A Cook and A E Cohen *J. Phys. Chem. A* **113** 6213 (2009)
- [10] A Cohen and Y Q Tang *J. Phys. Chem. A* **113** 9759 (2009)
- [11] Y Zhou, T Lei, L Wang, J Pei, Y Cao and J Wang *Adv. Mater.* **22** 1484 (2010)
- [12] D J Morrison, T K Trefz, W E Piers, R McDonald and M Parvez *J. Org. Chem.* **70** 5309 (2005)
- [13] H Gorner, C Stammel and J Mattay, *J. Photochem. Photobiol. A* **120** 171 (1999)
- [14] S Sahasithiwat, T Mophuang, L Menbangpung, S Kamtonwong and T Sooksimuang *Synth. Met.*, **160** 1148 (2010)
- [15] T Verbiest et al. *Science* **282** 913 (1998)
- [16] K E S Phillips, T J Katz, S Jockusch, A J Lovinger and N J Turro *J. Am. Chem. Soc.* **123** 11899 (2001)
- [17] S Van Elshocht et al. *Chem. Phys. Lett.* **323** 340 (2000)
- [18] M Siltanen, E Vuorimaa, H Lemmetyinen, P Ihalainen, J Peltonen and M Kauranen *J. Phys. Chem. B* **112** 1940 (2008)
- [19] E Murguly, R McDonald and N R Branda *Org. Lett.* **2** 3169 (2000)
- [20] F Mayer and T Oppenheimer *Ber. Dtsch. Chem. Ges.* **51** 510 (1918)
- [21] F Mayer and T Oppenheimer *J. Chem. Soc.* **114i** 339 (1918)
- [22] J W Cook *J. Chem. Soc.* 2524 (1931)
- [23] C L Hewett *J. Chem. Soc.* 1286 (1938)
- [24] A O McIntosh, J M Robertson and V Vand *Nature* **169** 322 (1952)
- [25] M S Newman, W B Lutz and D Lednicer *J. Am. Chem. Soc.* **77** 3420 (1955)
- [26] V K Aggarwal and M F Wang *Chem. Commun.* 191 (1996)
- [27] B L Feringa *Acc. Chem. Res.* **34** 504 (2001)
- [28] N Takenaka, R Singh, Sarangthem and B Captain *Angew. Chem., Int. Ed.* **47** 9708 (2008)
- [29] R Amemiya, N Saito and M Yamaguchi *J. Org. Chem.* **73** 7137 (2008)
- [30] M B Groen, H Schadenberg and H Wynberg *J. Org. Chem.* **36** 2797 (1971)
- [31] T Caronna, M Catellani, S Luzzati, L Malpezzi, S V Meille, A Mele, C Richter and R. Sinisi *Chem. Mater.* **13** 3906 (2001)
- [32] U H F Bunz *Angew. Chem. Int. Ed.* **49** 5037 (2010)
- [33] H Tsuji, C Mitsui, L Ilies, Y Sato and E Nakamura *J. Am. Chem. Soc.* **129** 11902 (2007)
- [34] C Mitsui, J Soeda, K Miwa, H Tsuji, J Takeya and E Nakamura *J. Am. Chem. Soc.* **134** 5448 (2012)
- [35] M Nakano, K Niimi, E Miyazaki, I Osaka and K Takimiya *J. Org. Chem.* **77** 8099 (2012)
- [36] N Islam and A H Pandith *J. Mol. Model.* **20** 2535 (2014)
- [37] N Islam, S Niaz, T Manzoor and A H Pandith *Spectrochim. Acta, A*, **131** 461 (2014)
- [38] R H Martin and M Baes *Tetrahedron* **31** 2135 (1975)
- [39] K Mori, T Murase and M Fujita *Angew. Chem., Int. Ed.* **54** 6847 (2015)
- [40] J Larsen and K Bechgaard *Acta Chem. Scand.* **50** 71 (1996)
- [41] M Miyasaka, A Rajca, M Pink and S Rajca *J. Am. Chem. Soc.* **127** 13806 (2005)
- [42] T Iwasaki, Y Kohinata and H Nishide *Org. Lett.* **7** 755 (2005)
- [43] H R Talele, S. Sahoo and A V Bedekar *Org. Lett.* **14** 3166 (2012)
- [44] G M Upadhyay, H R Talele, S Sahoo and A V Bedekar *Tetrahedron Lett.* **55** 5394 (2014)
- [45] G M Upadhyay and A V Bedekar *Tetrahedron* **71** 5644 (2015)
- [46] M S Sundar and A V Bedekar, *Org. Lett.* **17** 5808 (2015)
- [47] M J Frisch et al. Gaussian 09, Revision E.01, Gaussian, Inc., Wallingford CT (2009)
- [48] T Yanai, D Tew and N Handy *Chem. Phys. Lett.* **393** 51 (2004)
- [49] A D McLean and G S Chandler *J. Chem. Phys.* **72** 5639 (1980)
- [50] R Dennington, T Keith and J Millam GaussView, Version 5, Semichem Inc., Shawnee Mission KS (2009)
- [51] F Trani, G Scalmani, G S Zheng, I Carnimeo, M J Frisch and V Barone *J. Chem. Theory Comput.* **7** 3304 (2011)
- [52] D M Chipman, *J. Chem. Phys.* **112** 5558 (2000)
- [53] E Cancès and B Mennucci *J. Chem. Phys.* **114** 4744 (2001)
- [54] E Cancès, B Mennucci and J Tomasi *J. Chem. Phys.* **107** 3032 (1997)
- [55] B Mennucci and J Tomasi *J. Chem. Phys.* **106** 5151 (1997)
- [56] Y Fu, W Shen and M Li *Macromol. Theory Simul.* **17** 385 (2008)
- [57] Supporting information (calculation of quantum mechanical descriptors)
- [58] R A Marcus *J. Chem. Phys.* **26** 867 (1957)
- [59] R A Marcus *J. Chem. Phys.* **26** 872 (1957)
- [60] B C Lin, C P Cheng, Z Q You and C P Hsu *J. Am. Chem. Soc.* **127** 66 (2005)
- [61] O Parisel, Y Ellinger and C Giessner *Chem. Phys. Lett.* **250** 178 (1996)
- [62] K M Ervin, I Anusiewicz, P Skurski, J Simons and W C Lineberger *J. Phys. Chem. A* **107** 8521 (2003)
- [63] H Sasabe and J Kido *Chem. Mater.* **23** 621 (2011)
- [64] N Islam and A H Pandith *J. Coord. Chem.* **67** 3288 (2014)
- [65] N Islam and S S Chimni *Comp. Theor. Chem.* **1086** 58 (2016)
- [66] J L Oudar and D S Chemla *J. Chem. Phys.* **66** 2664 (1977)
- [67] A H Pandith and N Islam *PLoS ONE* (2014) doi: [10.1371/journal.pone.0114125](https://doi.org/10.1371/journal.pone.0114125)